

Article

# Effect of Carbon Nanotubes on Chloride Penetration in Cement Mortars

Panagiota T. Dalla , Ilias K. Tragazikis, Dimitrios A. Exarchos, Konstantinos G. Dassios \* ,  
Nektaria M. Barkoula and Theodore E. Matikas

Department of Materials Science and Engineering, University of Ioannina, Dourouti University Campus, GR-45110 Ioannina, Greece; pan.dalla@yahoo.gr (P.T.D.); itragazik@cc.uoi.gr (I.K.T.); dexarch@cc.uoi.gr (D.A.E.); nbarkoul@cc.uoi.gr (N.M.B.); matikas@cc.uoi.gr (T.E.M.)

\* Correspondence: kdassios@uoi.gr

Received: 30 December 2018; Accepted: 1 March 2019; Published: 12 March 2019



**Abstract:** The study investigates the effect of carbon nanotubes on chloride penetration in nano-modified mortars and reports on the physical, electrical, and mechanical performance of the material. Mortars were artificially corroded and their surface electrical surface conductivity as well as flexural and compressive strength were measured. The influence of variable nanotube concentration in accelerated corrosion damage was evaluated. Nanotube concentration was found to significantly affect the permeability of the mortars; improvements in flexural and compressive response of mortars exposed to salt spray fog, compared to virgin specimens, were rationalized upon decreases in the apparent porosity of the materials due to filling of the pores with sodium chloride. Electrical resistivity was found to increase up to two orders of magnitude with respect to the surface value; above the percolation threshold, the property impressively increased up to five orders of magnitude.

**Keywords:** chloride diffusion; cement mortars; carbon nanotubes; mechanical properties; electrical properties

## 1. Introduction

Reinforced cement-based structures are expected to remain intact for long periods of time with minimum service requirements. This demands the development and usage of long-lasting building materials. Lately, there is increasing attention towards incorporating nanoparticles in building materials for improvement of their mechanical and electrical performance as well as endowment of multi-functionality to the structure [1–3]. Relevant studies have explored the use, in cement-based materials, of such nano-reinforcements such as nano-CaCO<sub>3</sub> [4], nano-SiO<sub>2</sub> [5], as well as carbon-nanofibers (CNFs) [2], graphene nano-platelets [6,7] and carbon-nanotubes (CNTs) [8,9]. It has been reported that homogeneously-dispersed nano-particles can fill inherent voids in cement structures, hence lowering the porosity and increasing their strength and durability [10]. On the other hand, poor design and supervision, unsuitable construction, insufficient materials selection and harsh environments can severely downgrade cement structures [11–13].

One of the major durability issues that the construction industry is facing globally is the materials' structural degradation [14–17]. This may lead to reductions in strength, reinforcement corrosion, as well as aesthetics issues, which would require early repair or replacement of the structure [18]. Corrosion, attacking mainly reinforcements via the pores in the material bulk, is primarily due to carbonation and chloride attack [12,19–22]. Dry environments favor corrosion because of carbonation and carbon oxide excess [23]. On the other hand, localized corrosion in different types of cement-based

structures exposed to marine environments may lead to premature structure failure due to chloride ingress through the net of the material pores or via ion incorporation in the mixture [12,24,25].

In concrete, the corrosion process is completed in two stages: In the initial corrosion initiation stage, chlorides penetrate the concrete without causing damage to the material. In the second stage, termed corrosion propagation stage, corrosion elements accumulate until the material's ultimate failure [12]. For concrete structures in marine environments, the service life is the sum of the durations of the two stages, while durability and serviceability of the structures depend greatly on the duration of the initiation stage [12]. A variety of methods are currently available in the literature for prevention of deterioration due to chloride penetration, as are models for prediction of the time of corrosion initiation and total service life [19–24,26]. In order to better assess the phenomenon, knowledge of the different driving forces responsible for the penetration of chloride ions in concrete is indispensable. Possible such driving forces include absorption during wetting and drying cycles [27] and application of hydrostatic pressure, by means of an hydraulic head on the surface of the concrete [18]. However, the most common way in which chloride ions get in contact with concrete reinforcement is diffusion, *i.e.* the movement of chloride ions under a concentration gradient via a continuous liquid phase [28]. The penetration rate depends on the quality of the concrete, its chloride binding capacity, hydration degree, duration of exposure to chlorides, water to cement ratio, temperature and curing time, as well as the presence of supplementary cementing materials [12,18,24,28,29]. A sufficient understanding of these factors and their relationships could provide a good base for the limitation of degradation of cement-based structures.

The degree of resistance of concrete to chloride ion penetration is characterized by the coefficient of diffusion in Fick's corresponding second law [30]. Its calculation requires exposure of the concrete sample to known concentrations of chloride solutions for specific durations followed by measurement of chlorides' concentration at successively larger depths. The values of chloride diffusion coefficient usually vary from  $10^{-13}$  m<sup>2</sup>/s to  $10^{-10}$  m<sup>2</sup>/s [31] in relation to the concrete properties such as w/cm ratio, the type and proportion of mineral admixtures and cement, the material's compaction and curing state, chloride exposure conditions, as well as the presence of cracks [32]. Currently available experimental methods for the determination of concrete's resistance to chloride ion penetration include the rapid chloride permeability test (RCPT) as shown by Marta Kosior—Kazberuk [33], the rapid chloride test (RCT) method, and the rapid chloride migration test (RMT) [10,34–39]. Probably the most straightforward way of measuring chloride penetration is to immerse the specimens under investigation in salty solutions with different concentrations for specific periods of time depending on the needs of the experiment [40–42]. Ming Jin et al. suggested the measurement of electrical resistivity as a non-destructive method for monitoring chloride ion penetration in concrete structures by means of the electrical properties of graphene-modified cement composites [6].

While considerable research efforts have dealt with concrete behavior with respect to chloride penetration [10,16,38,39,43] and the effect of sodium chloride in mortars [42,44], there is currently a clear lack of knowledge on the effect of carbon nanotube (CNT) presence on chloride penetration in state-of-the-art nano-modified mortars intended for future exploitation in real constructions. The main purpose of the present study is to address the effect of chloride penetration in carbon nanotube-modified cementitious materials subjected to marine environments. For that reason, two different methods, namely the rapid chloride test method (RCT) and the rapid chloride permeability test method (RCPT) were used for the degradation of the specimens, while the mechanical and electrical behavior of the corroded materials was investigated.

## 2. Experimental Procedures

### 2.1. Materials and Specimens

Five cement mixtures of varying carbon nanotube concentrations, namely 0.2%, 0.4%, 0.6%, and 0.8% by weight of cement, were prepared according to standard protocol

“BS EN 196-1:2005” [45] pertaining to the determination of physical, mechanical, and electrical properties as well as chloride content in cement. A reference mixture without nano-inclusions was also prepared for comparison purposes. All mixtures contained ordinary Portland cement, regular tap water and natural sand. Long multi-wall carbon nanotubes (MWCNT), synthesized via catalytic chemical vapor deposition were used as nano-reinforcements. The tubes, commercially available by Shenzhen Nanotech Port Co. Ltd. (Shenzhen, China), had nominal purity higher than 97% and amorphous carbon content which is less than 3%. Nominal tube diameter ranged from 20 to 40 nm, while their length ranged from 5 to 15  $\mu\text{m}$ . Viscocrete Ultra 300 (Sika AG, Baar, Switzerland), which is a native water-based concrete additive comprised of polycarboxylate polymers, doubled as a superplasticizer and nanotube dispersing agent. Superplasticizer selection was based on its high CNT dispersion efficiency [8,46], excellent resistance to mechanical and chemical attack, as well as its ability to inhibit air entrapment inside the specimens. A second superplasticizer, Viscocrete Ultra 600 (Sika AG, Baar, Switzerland) was added in all fresh mortars, in amounts of approximately 1.5 g, to aid air content stability and workability, hence eliminating contributions of these phenomena to the overall behavior and enabling attribution of findings exclusively to nanotube concentration. In all cases, water to cement ratio was maintained at 0.5.

The experimental procedure for the preparation of nano-reinforced cement mixtures, at tube loadings of 0.2%, 0.4%, 0.6%, and 0.8 wt. % of cement, adopted the three following successive steps. Initially, the superplasticizer and nanotubes were mixed at a ratio of 1.5:1 under magnetic stirring, in regular tap water. Given the fact that for a single mix, BS EN 196-1 requires usage of 1350 g of sand, 450 g of cement, and 225 g of water, the relevant water/CNT ratios were 250 at 0.2% CNT concentration and 125%, 83.5%, and 62.5% at 0.4%, at 0.6%, and 0.8% CNT concentration, respectively. Accordingly, the sand/cement ratio was constant at 3:1. The resultant aqueous suspensions of MWCNTs were ultrasonicated for 90 min at room temperature with a Hielscher UP400S device (Hielscher Ultrasonics GmbH, Teltow, Germany) equipped with a cylindrical 22 mm diameter sonotrode delivering a power throughput of 4500 J/min at a frequency of 24 kHz. The selected combination of ultrasonication duration and energy rate was established as optimum for the suspension homogeneity achievement without tube aspect ratio impairment [47]. The ultrasonicated suspensions were mixed with ordinary Portland cement type “I 42.5N” and natural sand using a laboratory rotary mixer, in low and high speeds sequentially for a total of 4 min, according to standard test method BS EN 196-1:2005 [45]. Immediately after mixing, the workability and air content of the fresh mortars were measured. The remaining fresh mixture was poured into oiled metallic molds with internal dimensions of 40  $\times$  40  $\times$  160 mm for flexural and compressive test specimen production and 150  $\times$  150  $\times$  150 mm for chloride penetration and electrical conductivity measurement specimen, where they were left for 24 h before demolding. The specimens were subsequently placed into a 100% humidity room for 28 days before being transferred into a laboratory corrosive environment.

## 2.2. Properties in Fresh Conditions

Fresh mortar consistency was determined following flow table tests, carried out according to European Standard BS EN 1015-3:1999 [48]. Consistency is a measure of the fluidity and/or wetness of the fresh mortar and is indicative of the deformability of the fresh mortar when subjected to certain types of stresses [48]. The mortar was introduced into the mold carefully in two layers while excess mortar was removed. Subsequently, the mold was slowly raised, and the mortar was spread out on the flow table disc by jolting the table 15 times, approximately one per second. This causes the mortar to spread further, in a roughly circular shape. The flow diameter is the average of the maximum diameter of the pool of fresh mortar and the diameter at right angles. This average diameter value constitute the flowability of the mixture after subtraction of the mold diameter, 100 mm [48]. Mixture air content was determined after European Standard BS EN 1015-7:1999 [49]. Therein, using an air entrainment meter for mortars (TESTING Bluhm & Feuerherdt GmbH—Berlin, Germany), filling capacity of 1 L, water was introduced on top of the mortar surface and forced into the mortar by means of applied

air-pressure hence displacing air from within the pores. The corresponding drop in water level reflects the volume of air displaced from the mortar with the direct reading of the air content in percentage.

### 2.3. Chloride Penetration

The resistance to chloride penetration of the modified mortars with different CNT loadings was qualitatively evaluated using two effective methods, namely RCPT and RCT, suitable for concrete characterization. The specimens used in these tests were the cores of  $150 \times 150 \times 150 \text{ mm}^3$  cubic samples.

#### 2.3.1. RCPT Method

Rapid chloride ion penetrability test (RCPT) was conducted according to ASTM C1202-97 [50] using the PROOVE'it<sup>®</sup> system (Germann Instruments—Copenhagen, Denmark). It monitors the amount of electrical current passed through a 50 mm thick, 100 mm in diameter specimen, which was positioned in a measuring cell and supplied with a direct current (DC) electric current of 60 V for 6 h; the relevant apparatus is illustrated in Figure 1. In each side of the specimen rested a fluid reservoir. One reservoir was filled with 3% NaCl and was connected to the negative terminal, while the other was filled with  $0.3 \text{ mol/dm}^3$  solution of NaOH and was connected to the positive terminal of the power supply.

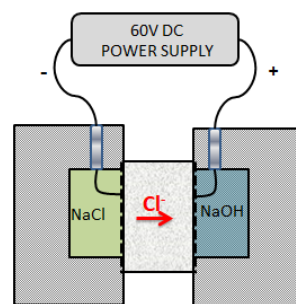


**Figure 1.** Experimental set up for the rapid chloride permeability test method.

The total charge, in Cb, passing through the specimen is representative of its resistance to chloride ion penetration. The chloride ion penetrability is evaluated qualitatively according to Table 1.

**Table 1.** Chloride ion penetrability based on charge passed.

Charge Passed [Cb]	Chloride Ion Penetrability
>4000	high
2000 ÷ 4000	moderate
1000 ÷ 2000	low
100 ÷ 1000	very low
<100	negligible

During the test, the solution temperature was monitored and maintained in the range of 20 to 25 °C, as higher temperatures aid acceleration of chloride ion transport, hence resulting in non-representative data.

#### 2.3.2. RCT Method

Evaluation of the chloride penetration features of nano-modified mortars was also carried out by exposing specimens to salt spray environments according to ASTM B117 [51] specifications. As laboratory conditions are much more aggressive than natural ones, to accelerate the phenomenon, severe corrosion states in short times were anticipated. Compared to other laboratory-grade

accelerated corrosion tests, the salt spray test was considered more representative of the natural coastal environment [52]. Therein, after removal from the 100% humidity room, nano-modified mortars were surface dried and then naturally dried in the laboratory environment. Subsequently, they were sealed with insulating exterior paint on four sides, including the top side of the mold and two opposite open sides permitted chloride diffusion through a predefined path. Coated samples were placed in a VSC 450 salt spray corrosion test chamber (Vötsch Industrietechnik, Balingen, Germany) (Figure 2a) for 100 days, with a sealed side resting at the bottom of the chamber (Figure 2b).



**Figure 2.** (a) Salt spray chamber and (b) sealed specimens inside the chamber.

Salt solution prepared by dissolving five parts, by mass, of sodium chloride (NaCl) into 95 parts of deionized water, was introduced into the chamber's solution reservoir. The utilized salt contained less than 0.3 percent impurities to avoid impurities acting as corrosion inhibitors. Salt spray solution acidity, measured at 25 °C, was maintained in the pH range from 6.5 to 7.2, while the temperature inside the chamber was maintained at 35 °C [52]. After the end of the 100-day exposure period, nano-reinforced mortars were carefully removed from the chamber and gently washed with clean tap water to remove any surface salt deposit before being naturally dried.

The dried mortars were prepared for testing by the following methodology. Initially, a cylindrical core of the exposed sides to the NaCl was drilled out of each cubic specimen. The diameter of the cores was maintained within 95 mm to 105 mm while sectioning of the total length provided cylindrical samples of an approximate height of about 65 mm, such as the ones shown in Figure 3.

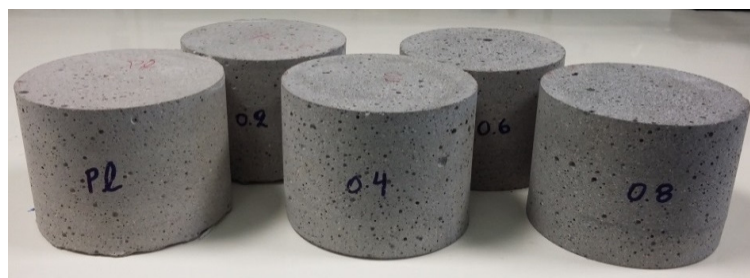


**Figure 3.** Testing cores drilled off from mortars exposed to accelerated corrosion.

Subsequently, 1.5 g of powder ground from incrementally increasing depths inside the nano-modified material were removed using a profile grinder (Germann Instruments—Copenhagen, Denmark) and collected for chloride ion measurement. The grinding depth increment was kept as low as 1 mm, to allow for high accuracy measurement; 60 successive depths were interrogated. Next, ground powders originating from mortars with different CNT content were tested separately according to the rapid chloride test (RCT) method. In this way, the amount of chloride calculated using the RCT

electrode, which was initially calibrated, was related to CNT loading. Profiles of chloride content versus the depth below the exposed surface were determined.

Assuming that diffusion is a one dimensional process, diffusion of chloride ions into the materials is governed by Fick's second law of diffusion (steady state diffusion) as follows:

$$\frac{\partial C(x)}{\partial t} = D \frac{\partial^2 C}{\partial x^2} \quad (1)$$

where C represents chloride ion concentration, x is the depth from the surface of concrete, t represents time, and D is the diffusion coefficient.

Solving Equation (1) requires knowledge of initial and boundary conditions as well as the value of the diffusion coefficient, D. For a constant diffusion coefficient and under the assumptions that chloride ion concentration on the material's surface is constant ( $C_s = C(0,t)$ ), the initial concentration ( $C_i$ ) is zero and the concentration at an infinite point, quite deep in relation to the surface, is also zero. Equation (1) converts to Crank's solution [53] as follows:

$$C(x, t) = C_s - (C_s - C_i) \operatorname{erf} \left( \frac{x}{2\sqrt{Dt}} \right) \quad (2)$$

where  $C(x,t)$  indicates the chloride ion concentration at a depth of x, measured from the surface in mm, at an elapsed time t, measured in years, from the start of the chloride exposure

$C_s$  is the chloride concentration (% of materials mass) at the material's surface

$C_i$  is the initial or background chloride concentration (% of materials mass)

D represents the chloride diffusion coefficient ( $\text{mm}^2/\text{year}$ )

Equation (2) describes the variation of chloride ion content as a function of the distance x from the surface of the sample, after an elapsed time t since initial exposure to a constant surface chloride concentration of  $C_s$ . The values of parameters  $C_s$  and D are determined using the least-squares curve fitting that permits general non-linear regression analysis.

#### 2.4. Porosimetry

The pore structure of the mortars modified with variable nanotube concentrations was analyzed by mercury porosimetry in a PoreMaster 60 porosimeter (Quantachrome GmbH & Co. KG, Odelzhausen, Germany). The measurements were performed on small nano-modified mortar volumes, less than  $1 \text{ cm}^3$ , extracted from specimens after mechanical testing failure.

#### 2.5. Electrical Conductivity Measurements

Surface electrical conductivity was incrementally measured at the exposed mortar surface, after step grinding of 10 mm of material. DC electrical conductivity was measured using a custom-built contact electrical conductivity probe connected to an ultra-high precision digital electrometer/high resistance meter (Keithley 6517B, Tektronix Inc., Beaverton, OR, USA) capable of measuring resistances up to 1018 with a  $10 \times 10^{-18} \text{ A}$  current resolution. The probe, presented in detail in reference [2], consists of a circular head comprised of 22 concentrically-arranged spring-loaded pin electrodes with conductive rubber ends for optimal contact with the non-planar cement surfaces. The head rested on a z-translational stage, which could be lowered and brought into contact with the specimen at constant force by means of a lever. Conductivity, assumed exclusively attributable to nanotube presence, is anticipated to vary with interrogation depth as a result of variable chloride ion concentration at the instant depth.

#### 2.6. Mechanical Performance

Mechanical characterization of corroded nano-modified mortars under the four point bending test configuration was performed on  $40 \times 40 \times 160 \text{ mm}^3$  specimens on an Instron 5967 testing frame

(Instron, Norwood, MA, USA) equipped with a 30 kN loadcell according to standard test protocol ASTM C1609 [54]. Prism halves occurring after the catastrophic bending test, were subjected to compression testing, at a load rate of 2400 N/s, which corresponds to a stress rate of 1.5 MPa/s for the 40x40 mm<sup>2</sup> tested area, following the standard protocol EN 196-1:2005 [41].

### 3. Results and Discussion

#### 3.1. Workability and Air Content of Fresh Mortars

Fresh mortar properties are the ones which determine the application range of the material. During the course of the present study, workability as well as air content of the fresh nano-reinforced mortars was maintained, in similar values throughout mixtures of variable nanotube concentration, by addition of differential amounts of Viscocrete 600 superplasticizer as needed. As can be observed in Figure 4, the workability of the mortars reinforced with different concentrations of carbon nanotubes does not vary significantly from the starting, plain-mortar value. It must be recalled that the sole dispersion assistive agent used in the mixture, which affects workability, was Viscocrete Ultra 300, a native concrete additive which has proven highly effective for CNT dispersion, hence rendering surfactant usage and chemical tube functionalization, unnecessary [8,55]. The invariance of workability with respect to tube loading is a favorable finding, it ensures that the latter can act as the sole parameter responsible for any documented variation in properties.

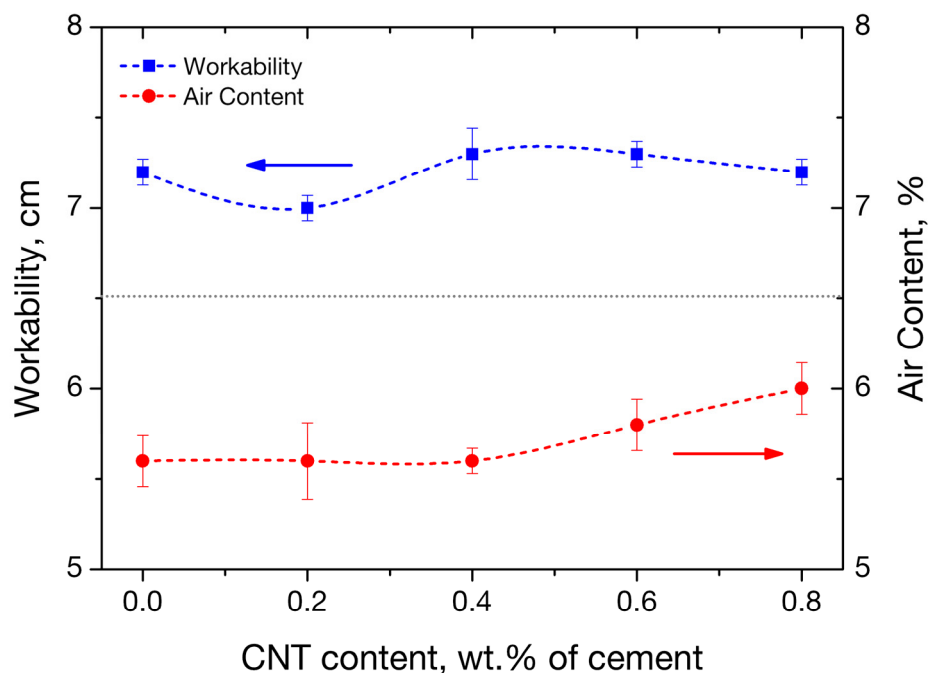


**Figure 4.** Change of flowability and air content across nano-modified mortars with different concentrations of carbon nanotubes.

Following completion of the flow table test, proper volumes of fresh mortars were used for air content testing. Results from each mixture are plotted as a function of the tube content in Figure 4. Here again, all specimens are observed to share similar air contents, a finding which confirms the workability results as well as the role of Viscocrete 600 superplasticizer in the mixing procedure.

### 3.2. Chloride Profile of the CNTs Nano-Modified Mortars

#### 3.2.1. RCPT Method

The resistance to chloride penetration was initially evaluated qualitatively using the RCPT method; results of current passing through nano-modified mortars with different CNT loadings after curing duration of 28 days are illustrated in Figure 5. It is therein observed that throughout the whole test duration, current was lower for plain specimens and increased with CNT concentration. The current passing through the sample with 0.8% wt. CNTs was approximately 20% higher than in the sample with no nano-reinforcement. The observed behavior is rationalized upon the anticipated increase in conductivity endowed by higher concentrations of the conductive filler and compares favorably to relevant recent findings [56,57]

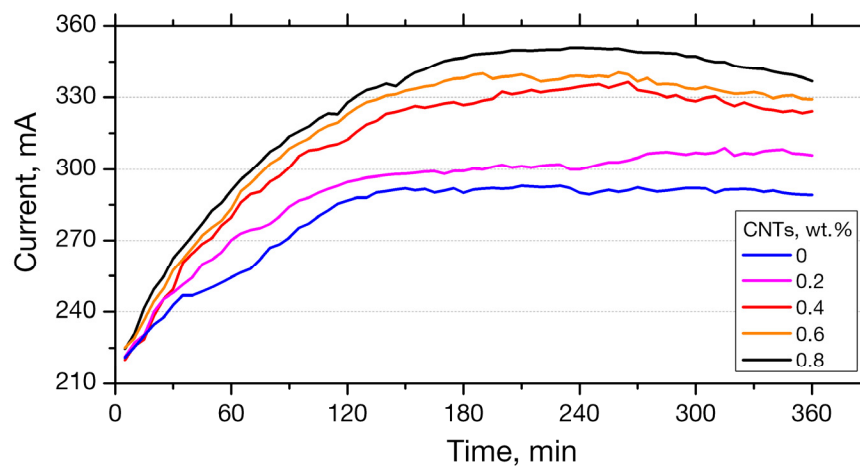


**Figure 5.** Current passing through nano-modified mortars with different amount of carbon nanotubes (CNTs).

The electric charge allowed to pass through the nano-modified mortars is illustrated in Figure 6 as a function of tube concentration. Therein, negligible charge variation is observed with CNT loading, while according to Table 1 classification, all samples appear to exhibit high chloride ion penetrability. Furthermore, it is shown that the charge passing through the plain specimens is almost identical to that passing through nano-modified mortars, a finding which suggests complete invariance of the particular behavior to carbon nanotube presence. In view of these findings, three factors in the RCPT method must not be neglected: (i) That the current passed is related to all ions in the pore solution, not just chloride ions, (ii) that measurements are taken before steady-state migration is achieved, and (iii) that the high voltage applied may lead to temperature increase which, in turn, may influence the measurement [18,28].

#### 3.2.2. RCT Method

As aforementioned, following 100 day exposure to salt spray, profile grinding at an increment of 1 mm, a total of 60 interrogations were performed. Figure 7 plots the typical chloride concentration profiles, expressed in % mass of mortar as a function of interrogation depth.

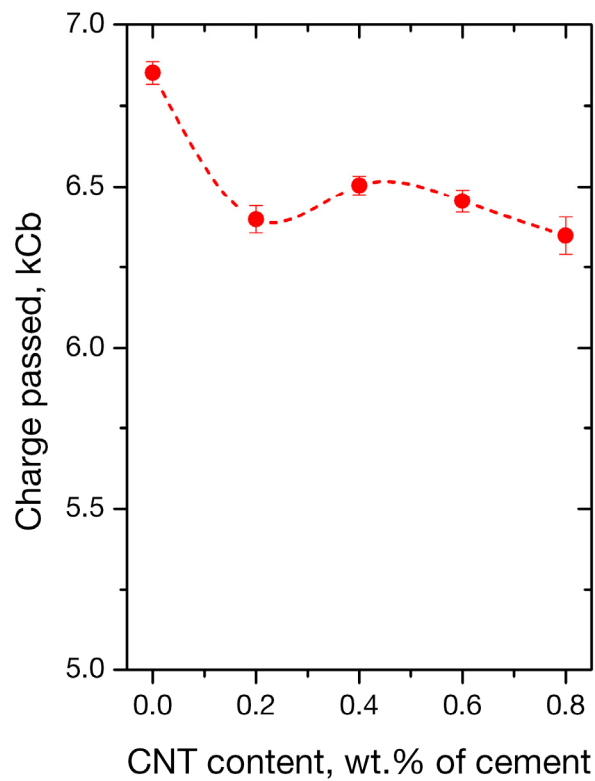


Figure 6. Total charge passed through specimens with different CNT loadings.

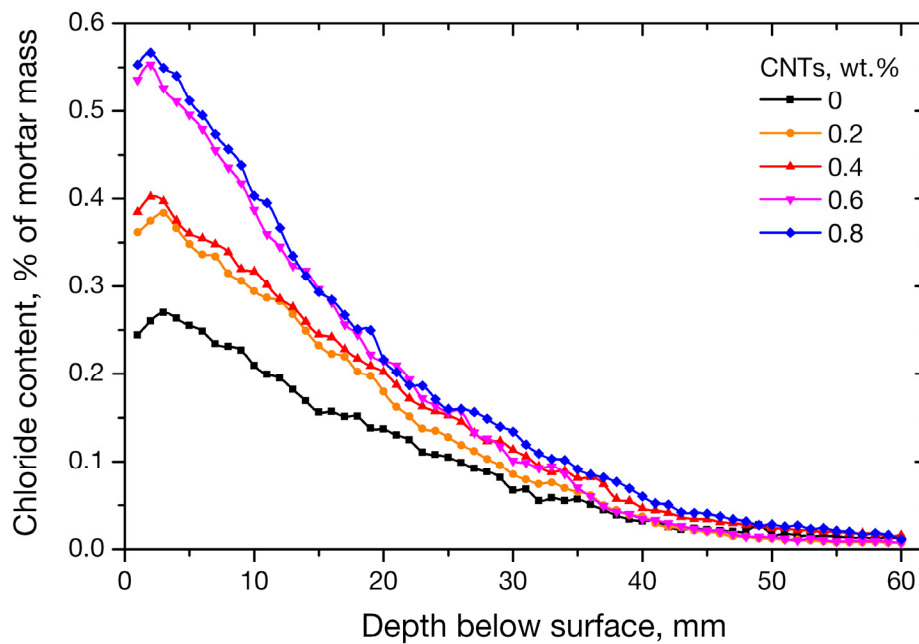
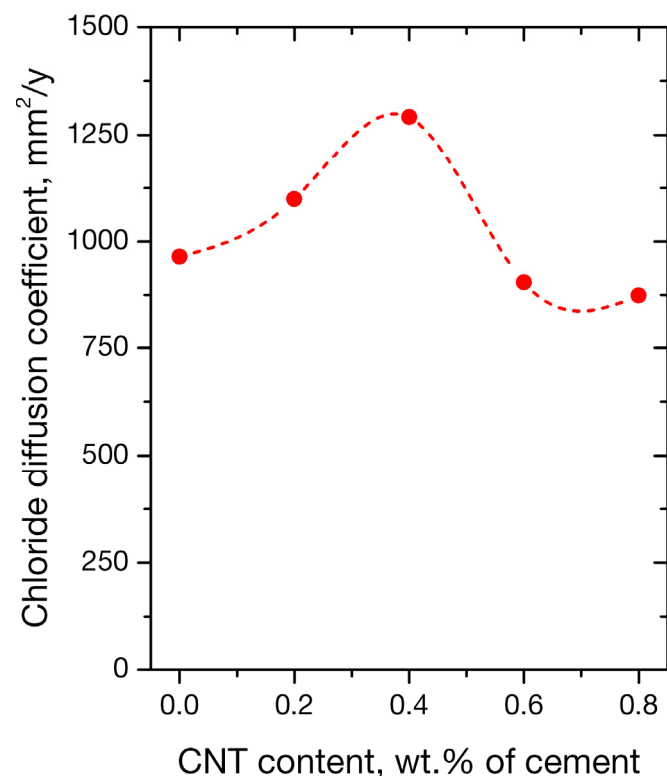


Figure 7. Chloride profile of the nano-modified mortars at different depths.

It is observed that the profiles had an almost identical shape throughout mortars of variable CNT concentration, with chloride content being at a maximum near the surface and decreasing with interrogation depth. For all specimens, the first one or two measurements, corresponding to the first two grinding steps, show less chloride ions than expected as a result of the aforementioned washout, which was performed following the exposure procedure [58]. These initial data points were not considered in the least-squares regression analysis for the obtainment of the best-fit values of the parameters of Equation (2). Moreover, it is observed that after the first 50 mm below the exposed

surface, ion content drops to less than 0.05% where nanotube presence does not make a difference to the total recorded behavior. Most importantly, at all depths, chloride content was consistently higher for samples with higher CNT concentrations, a finding which signifies that chloride ion concentration is directly affected by nanotube presence. According to Figure 7, the influence is moderate for CNT loadings of 0.2% and 0.4% wt. of cement and more intense in mortars loaded with 0.6% and 0.8% nanotubes. Chloride concentration in mortars with 0.8% wt. cement CNTs is almost 50% higher than that of plain mortars. It is believed that after drying the mortars that were exposed to salt spray, chloride ions are still present in the cement matrix, although the network of pore water which initially carried them and acted as an electrical pathway, is now removed. Resultant chloride-containing crystals are electrically conductive and are now precipitated between networks of conducting carbon nanotubes. This facilitates electrical current flow through the material and absorption of a considerable amount of chloride ions. Inarguably, bigger amounts of chloride ions manage to travel effectively and are trapped to the inner part of the structure as CNT concentration increases. The chloride diffusion coefficient values calculated for nano-modified mortars exposed to 5% NaCl solution following the analysis presented in Section 2.3.2 are shown in Figure 8. It is therein observed that the coefficient increases for the first two nanotube loadings and is at a maximum at a CNT concentration of 0.4% wt. of cement above which it drops again by approximately 30% of the maximum value, to the level of the plain specimens or slightly lower. Joining information from Figures 7 and 8, it can be argued that higher chloride diffusion coefficient values do not necessarily signify larger amounts of chlorides penetration in the specimen. This is because the coefficient expresses how fast the chlorides are transported in the material and depends on external factors such as the degree of hydration and saturation, as well as porosity.



**Figure 8.** Chloride diffusion coefficient for each nano-modified mortar.

### 3.3. Porosity

The pore size distributions measured by mercury porosimetry in mortars with variable carbon nanotube contents are presented in Figure 9. It is therein observed that all mortars exhibited overall comparable pore distribution curves with the main features being (i) the dominant peak at ca.

$6 \times 10^{-3} \mu\text{m}$ , on 6 nm, which is fixed throughout variable nano-inclusion concentrations and is inarguably attributed to intra-nanotube porosity, i.e., the over volume corresponding to the internal open space of the cylindrical multi-walled tubes, and (ii) a pore range of non-consistent peaks up to  $0.2 \mu\text{m}$ .

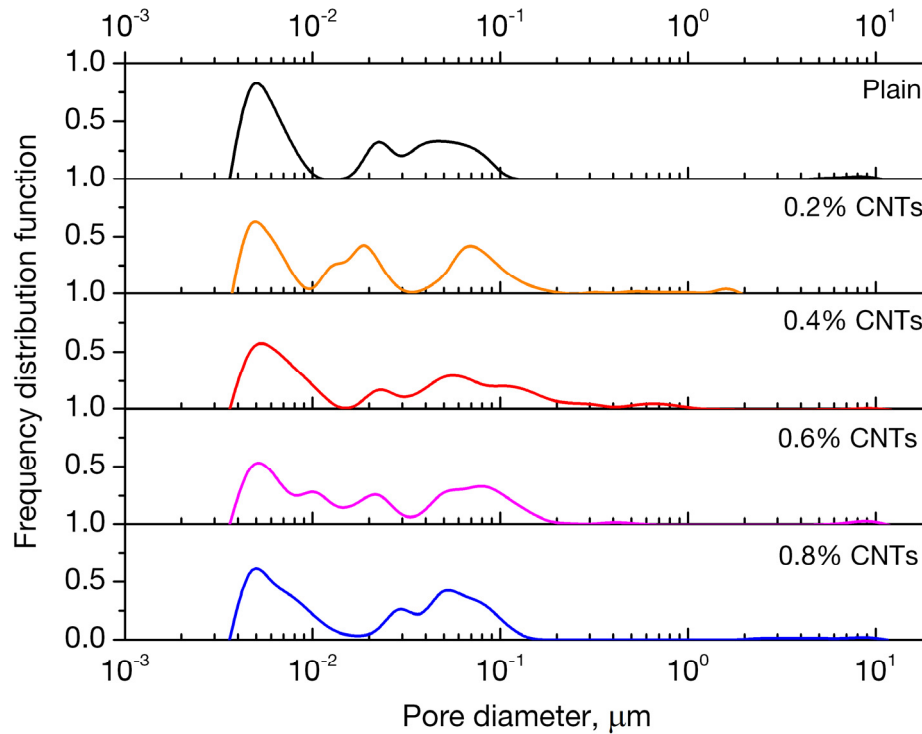


Figure 9. Pore size distributions of nano-modified mortars.

The actual porosity values for each mortar with variable CNT concentration are given in Table 2. It is observed that the total porosity drops with an increasing CNT concentration up to 0.4 wt. %, above which it increases to values even higher than the plain case. This may be due to nanotube entanglement issues at higher nano-inclusion concentrations.

Table 2. Porosity values for nano-modified mortars.

CNT Content % wt. of Cement	Porosity (%)
0	16.22
0.2	14.64
0.4	12.68
0.6	19.28
0.8	20.57

Additionally, chloride diffusion coefficients of corroded mortars are plotted as a function of respective mortar porosity in Figure 10. An inverse correlation between the two parameters is therein observed, with diffusion coefficients values decreasing with total porosity. This finding can be rationalized upon considering that more porous microstructures can block the rate of chloride penetration inside the testing mortars.

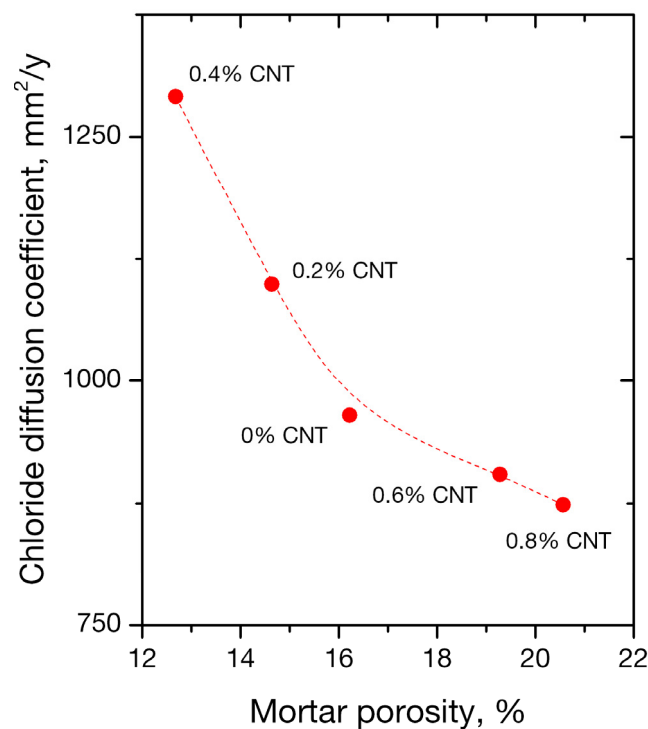


**Figure 10.** Chloride diffusion coefficient a function of mortar porosity.

Based on the above results, chloride diffusion in the processed mortars appears to be strongly linked with CNT concentration. This is due to a combination of mechanisms, one related to the raise of electric conductivity for CNT concentrations above the percolation threshold [2], the other associated to the fact that CNT addition lowers porosity values in the material. Hence, CNTs affect chloride diffusivity both directly, by affecting electrical transport properties, but also indirectly, by affecting the microstructure.

#### 3.4. Electrical Properties of Nano-Modified Mortars

The effect of salt spray (fog) corrosion test on the mortars' electrical properties was investigated by measurement of surface electrical resistivity at successive depths inside the ground mortars, with a step of 10 mm, as shown in Figure 11. The depicted changes in electrical resistivity at successive depths below the exposed surface are indicative of physical and chemical changes taking place into the material [33]. Specimens with 0%, 0.2% and 0.4% nano-inclusion concentrations, demonstrate a gradual increase in surface electrical resistivity with interrogation depth and reach, at a depth of 60 mm, a practically common value. This indicates the absence of chloride ions at such depths, independently of the concentration of nano-inclusions in the compositions. On the other hand, resistivity in samples with 0.6% and 0.8% nano-inclusion concentrations commences at the surface with significantly lower values than in the previous case, and follows a gradually increasing trend with depth, until it catches up with the behavior of the lower CNT concentrations. This may be attributed to the electrical percolation threshold of the nano-modified mortars wherein a conductive filler concentration of 0.6% wt. cement CNTs is already sufficient for the creation of a conductive electrical path [2]. Electrical resistivity appears to increase with interrogation depth below the exposed surface, which indicates that chloride concentration decreases with depth. On the contrary, porosity is one of the main parameters affecting the electrical resistivity in a cement-based material. The lower porosity values of specimens with 0.6% and 0.8% wt. to cement carbon nanotubes (Table 2), may indicate that the electrical current takes the path of least resistance inside the specific structures.

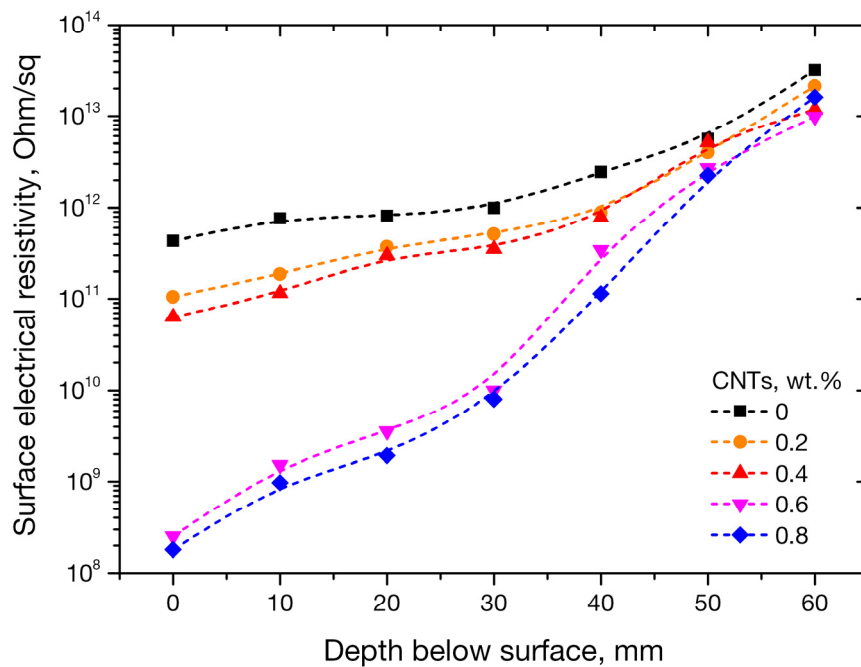


**Figure 11.** Surface electrical resistivity with respect to the depth below the exposed surface for all the nano-modified cement mortar.

### 3.5. Mechanical Performance of Nano-Modified Mortars

The effect of carbon nanotube concentration on the flexural and compressive strengths of the nano-modified mortars, both before and after exposure to salt spray conditions for a duration of 100 days, is presented in Figure 12. Virgin samples exhibited negligible fluctuation of the compressive strength with respect to CNT content, while flexural strength showed a small increase up to 0.4% CNT loadings. These findings compare favorably with previous research dedicated to the mechanical properties of CNT-modified mortars [8]. It is observed that exposure to sea fog resulted in improved flexural and mechanical properties for all specimens, irrespective of nanotube concentration. Concerning flexural strength, the property appears to increase by approximately 10%, commonly for mortars with CNT concentrations up to 0.4 wt. %, as a result of exposure to NaCl. The highest increase with respect to unexposed specimens is 22% and is noted for mortars with 0.8 wt. % nanotube content. These results are not incompatible with the porosimetry findings, wherein the inner pores of the specimens are filled with salt from the water solution that mortars are subjected to. Because of the lower porosity of the specimens with 0.6% and 0.8%, the percent increase of flexural strength of the specimens up to 0.4% nanotube concentration is greater. On the other hand, compressive strength appears to increase after the exposure to salt spray conditions for all the investigated ranges of carbon nanotube loadings and is generally constant at about 10%.

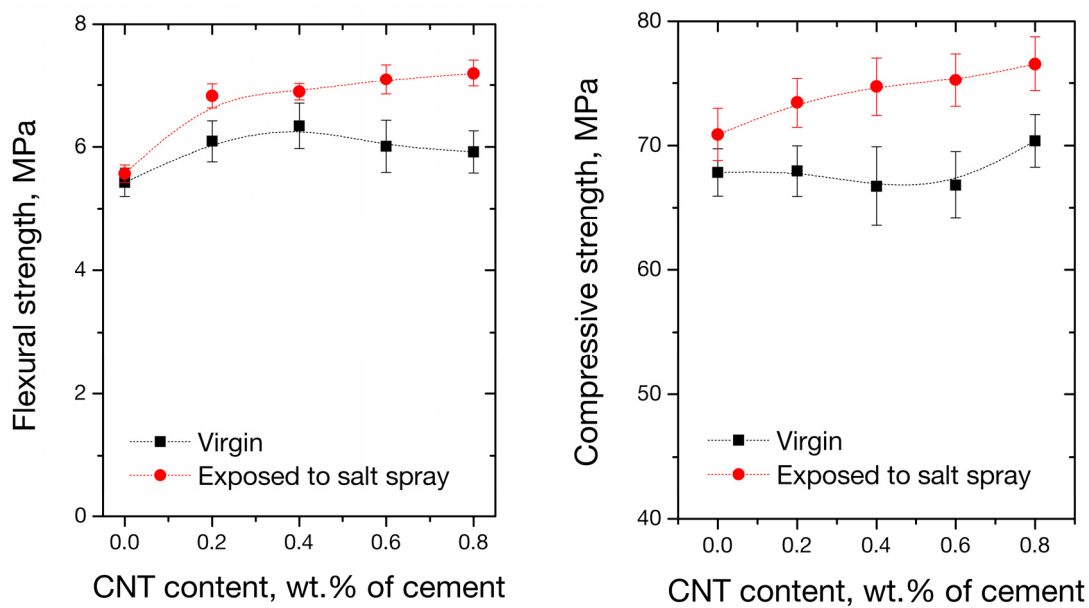


**Figure 12.** Mechanical properties of the nano-modified mortars before and after the exposure to the salt spray chamber.

#### 4. Conclusions

The effect of carbon nanotube concentration on chloride penetration in nano-modified mortars was investigated, and their physical, electrical, and mechanical performance were assessed. Mortar workability and air content in fresh conditions were kept constant among variable nanofiller concentrations, thus as to not influence the ion penetration inside the nano-modified specimens, and allow for rationalization of the findings by means of variable nanotube loading, exclusively. The main conclusions can be summarized as follows:

1. Using the rapid chloride permeability test method (RCPT) for plain and nano-reinforced mortars, all mortars were observed to exhibit high ion permeability. It must not be neglected that the RCPT-measurable permeability reflects not only chloride ions, but the total of ions contained to the mixture.
2. Nano-inclusions were found to affect the permeability of the mortars since the absorbed ion chlorides increased with nanotube concentration. Diffusion coefficient ( $D_a$ ) did not follow the same trend; it increased up to 0.4 wt. % of nanofiller content and decreased for higher contents of 0.6% and 0.8%. Porosimetry findings are compatible with the observed behavior.
3. The flexural and compressive properties of mortars exposed to salt spray fog present improved values compared to the virgin specimens. The observed improvement was rationalized upon sodium chloride filling the pores, which resulted in a decrease in apparent porosity and an increase in material strength.
4. Electrical resistivity, measured incrementally every 10 mm below the surface of the specimen, presented notable variations as a result of the specimens' subjection to NaCl solution. For mortars with 0, 0.2, and 0.4 wt. % CNTs, resistivity increased up to two orders of magnitude with interrogation depth. On the other hand, mortars with percolated conductive nanofiller networks at CNT concentrations of 0.6 and 0.8 wt. % CNTs, exhibited increases in electrical resistivity up to five orders of magnitude with respect to the surface value.

**Author Contributions:** Conceptualization, K.G.D. and T.E.M.; methodology, K.G.D., N.M.B., and T.E.M.; validation, P.T.D., I.K.T., and D.A.E.; formal analysis, P.T.D., I.K.T., D.A.E. and N.M.B.; investigation, P.T.D., I.K.T., D.A.E., and N.M.B.; data curation, P.T.D., I.K.T., D.A.E. and N.M.B.; writing—original draft preparation, P.T.D. and K.G.D.; writing—review and editing, P.T.D. and K.G.D.; visualization, X.X.; supervision, K.G.D., N.M.B. and T.E.M.; project administration, K.G.D. and T.E.M.

**Funding:** This research received no external funding.

**Conflicts of Interest:** The authors declare no conflict of interest.

## References

- Sanchez, F.; Sobolev, K. Nanotechnology in concrete—A review. *Constr. Build. Mater.* **2010**, *24*, 2060–2071. [[CrossRef](#)]
- Dalla, P.T.; Dassios, K.G.; Tragazikis, I.K.; Exarchos, D.A.; Matikas, T.E. Carbon nanotubes and nanofibers as strain and damage sensors for smart cement. *Mater. Today Commun.* **2016**, *8*, 196–204. [[CrossRef](#)]
- Tragazikis, I.; Dalla, P.; Exarchos, D.; Dassios, K.; Matikas, T. Nondestructive evaluation of the mechanical behavior of cement based nanocomposites under bending. *Proc. SPIE* **2015**, *9436*, 94360F.
- Kawashima, S.; Seo, J.-W.T.; Corr, D.; Hersam, M.C.; Shah, S.P. Dispersion of CaCO<sub>3</sub> nanoparticles by sonication and surfactant treatment for application in fly ash–cement systems. *Mater. Struct.* **2014**, *47*, 1011–1023. [[CrossRef](#)]
- Hou, P.; Qian, J.; Cheng, X.; Shah, S.P. Effects of the pozzolanic reactivity of nanoSiO<sub>2</sub> on cement-based materials. *Cem. Concr. Compos.* **2015**, *55*, 250–258. [[CrossRef](#)]
- Jin, M.; Jiang, L.; Lu, M.; Bai, S. Monitoring chloride ion penetration in concrete structure based on the conductivity of graphene/cement composite. *Constr. Build. Mater.* **2017**, *136*, 394–404. [[CrossRef](#)]
- Tragazikis, I.K.; Dassios, K.G.; Dalla, P.T.; Exarchos, D.A.; Matikas, T.E. Acoustic emission investigation of the effect of graphene on the fracture behavior of cement mortars. *Eng. Fract. Mech.* **2018**, in press. [[CrossRef](#)]
- Tragazikis, I.K.; Dassios, K.G.; Exarchos, D.A.; Dalla, P.T.; Matikas, T.E. Acoustic emission investigation of the mechanical performance of carbon nanotube-modified cement-based mortars. *Constr. Build. Mater.* **2016**, *122*, 518–524. [[CrossRef](#)]
- Dheeraj Swamy, B.L.P.; Raghavan, V.; Srinivas, K.; Narasinga Rao, K.; Lakshmanan, M.; Jayanarayanan, K.; Mini, K.M. Influence of silica based carbon nano tube composites in concrete. *Adv. Compos. Lett.* **2017**, *26*, 12–17.
- Du, H.; Gao, H.J.; Pang, S.D. Improvement in concrete resistance against water and chloride ingress by adding graphene nanoplatelet. *Cem. Concr. Res.* **2016**, *83*, 114–123. [[CrossRef](#)]
- Darmawan, M.S.; Bayuaji, R.; Husin, N.A.; Anugraha, R.B. Case Study of Remaining Service Life Assessment of a Cooling Water Intake Concrete Structure in Indonesia. *Adv. Civ. Eng.* **2014**, *2014*, 16. [[CrossRef](#)]
- Hodhod, O.A.; Ahmed, H.I. Modeling the service life of slag concrete exposed to chlorides. *Ain Shams Eng. J.* **2014**, *5*, 49–54. [[CrossRef](#)]
- Neville, A. Chloride attack of reinforced concrete: An overview. *Mater. Struct.* **1995**, *28*, 63. [[CrossRef](#)]
- Zhu, J.; Zhang, Y.; Zhao, D. Durability Assessment of an RC Railway Bridge Pier under a Chloride-Induced Corrosion Environment. In Proceedings of the Fifth International Conference on Transportation Engineering, Dalian, China, 26–27 September 2015.
- Zeng, L.; Song, R. Controlling chloride ions diffusion in concrete. *Sci. Rep.* **2013**, *3*, 3359. [[CrossRef](#)]
- Song, Z.; Jiang, L.; Liu, J.; Liu, J. Influence of cation type on diffusion behavior of chloride ions in concrete. *Constr. Build. Mater.* **2015**, *99*, 150–158. [[CrossRef](#)]
- Otieno, M.; Beushausen, H.; Alexander, M. Chloride-induced corrosion of steel in cracked concrete – Part I: Experimental studies under accelerated and natural marine environments. *Cem. Concr. Res.* **2016**, *79*, 373–385. [[CrossRef](#)]
- Stanish, K.D.; Hooton, R.D.; Thomas, M.D. *Testing the Chloride Penetration Resistance of Concrete: A Literature Review*; FHWA Contract DTFH61; Department of Civil Engineering, University of Toronto: Toronto, ON, Canada, 1997.
- Liang, M.T.; Wang, K.L.; Liang, C.H. Service life prediction of reinforced concrete structures. *Cem. Concr. Res.* **1999**, *29*, 1411–1418. [[CrossRef](#)]
- Liang, M.T.; Hong, C.L.; Liang, C.H. Service life prediction of existing reinforced concrete structures under carbonation-induced corrosion. *J. Chin. Inst. Civ. Hydraul. Eng.* **1999**, *11*, 485–492.
- Morinaga, S. *Prediction of Service Lives of Reinforced Concrete Buildings Based on Rate of Corrosion of Reinforcing Steel*; Report No. 23; Shimizu Corp: Tokyo, Japan, 1988; pp. 82–89.
- Jamali, A.; Angst, U.; Adey, B.; Elsener, B. Modeling of corrosion-induced concrete cover cracking: A critical analysis. *Constr. Build. Mater.* **2013**, *42*, 225–237. [[CrossRef](#)]

23. Ranjith, A.; Rao, K.B.; Manjunath, K. Evaluating the effect of corrosion on service life prediction of RC structures—A parametric study. *Int. J. Sustain. Built Environ.* **2016**, *5*, 587–603. [[CrossRef](#)]
24. Roa-Rodriguez, G.; Aperador, W.; Delgado, A. Calculation of Chloride Penetration Profile in Concrete Structures. *Int. J. Electrochem. Sci.* **2013**, *8*, 5022–5035.
25. Kim, H.K.; Jang, J.G.; Choi, Y.C.; Lee, H.K. Improved chloride resistance of high-strength concrete amended with coal bottom ash for internal curing. *Constr. Build. Mater.* **2014**, *71*, 334–343. [[CrossRef](#)]
26. Liang, M.T.; Huang, R.; Feng, S.A.; Yeh, C.J. Service life prediction of pier for the existing reinforced concrete bridges in chloride-laden environment. *J. Mar. Sci. Technol.* **2009**, *17*, 312–319.
27. Gergely, J.; Bledsoe, J.E.; Tempest, B.Q.; Szabo, I.F. *Concrete Diffusion Coefficients and Existing Chloride Exposure in North Carolina*; Project No. HWY-2004-12; Department of Civil Engineering, University of North Carolina at Charlotte: Charlotte, NC, USA, 2006.
28. Altaf Ahmad, A.K. Chloride ion migration/diffusion through concrete and test methods. *Int. J. Adv. Sci. Tech. Res.* **2013**, *6*, 151–180.
29. Angst, U.; Elsener, B.; Larsen, C.K.; Vennesland, Ø. Critical chloride content in reinforced concrete—A review. *Cem. Concr. Res.* **2009**, *39*, 1122–1138. [[CrossRef](#)]
30. Paul, A.; Laurila, T.; Vuorinen, V.; Divinski, S.V. Fick's Laws of Diffusion. In *Thermodynamics, Diffusion and the Kirkendall Effect in Solids*; Springer International Publishing: Cham, Switzerland, 2014; pp. 115–139.
31. Bertolini, L.; Elsener, B.; Pedferri, P.; Polder, R. *Corrosion of Steel in Concrete: Prevention, Diagnosis, Repair*; Wiley-VCH: Weinheim, Germany, 2004.
32. Shi, X.; Yang, Z.; Liu, Y.; Cross, D. Strength and corrosion properties of Portland cement mortar and concrete with mineral admixtures. *Constr. Build. Mater.* **2011**, *25*, 3245–3256. [[CrossRef](#)]
33. Kosior-Kazberuk, M.; Jezierski, W. Evaluation of concrete resistance to chloride ions penetration by means of electric resistivity monitoring. *J. Civ. Eng. Manag.* **2005**, *11*, 109–114. [[CrossRef](#)]
34. Liu, J.; Wang, X.; Qiu, Q.; Ou, G.; Xing, F. Understanding the effect of curing age on the chloride resistance of fly ash blended concrete by rapid chloride migration test. *Mater. Chem. Phys.* **2017**, *196*, 315–323. [[CrossRef](#)]
35. Dodds, W.; Christodoulou, C.; Goodier, C.; Austin, S.; Dunne, D. Durability performance of sustainable structural concrete: Effect of coarse crushed concrete aggregate on rapid chloride migration and accelerated corrosion. *Constr. Build. Mater.* **2017**, *155*, 511–521. [[CrossRef](#)]
36. Ying, J.; Zhou, B.; Xiao, J. Pore structure and chloride diffusivity of recycled aggregate concrete with nano-SiO<sub>2</sub> and nano-TiO<sub>2</sub>. *Constr. Build. Mater.* **2017**, *150*, 49–55. [[CrossRef](#)]
37. Snyder, K.A.; Ferraris, C.; Martys, N.S.; Garboczi, E.J. Using Impedance Spectroscopy to Assess the Viability of the Rapid Chloride Test for Determining Concrete Conductivity. *J. Res. Natl. Inst. Stand. Technol.* **2000**, *105*, 497–509. [[CrossRef](#)]
38. Valipour, M.; Shekarchi, M.; Arezoumandi, M. Chlorine diffusion resistivity of sustainable green concrete in harsh marine environments. *J. Clean. Prod.* **2017**, *142*, 4092–4100. [[CrossRef](#)]
39. Madani, H.; Bagheri, A.; Parhizkar, T.; Raisghasemi, A. Chloride penetration and electrical resistivity of concretes containing nanosilica hydrosols with different specific surface areas. *Cem. Concr. Compos.* **2014**, *53*, 18–24. [[CrossRef](#)]
40. Song, Z.; Jiang, L.; Zhang, Z.; Xiong, C. Distance-associated chloride binding capacity of cement paste subjected to natural diffusion. *Constr. Build. Mater.* **2016**, *112*, 925–932. [[CrossRef](#)]
41. Arya, C.; Buenfeld, N.R.; Newman, J.B. Factors influencing chloride-binding in concrete. *Cem. Concr. Res.* **1990**, *20*, 291–300. [[CrossRef](#)]
42. Kim, H.-K. Chloride penetration monitoring in reinforced concrete structure using carbon nanotube/cement composite. *Constr. Build. Mater.* **2015**, *96*, 29–36. [[CrossRef](#)]
43. Aldea, C.-M.; Young, F.; Wang, K.; Shah, S.P. Effects of curing conditions on properties of concrete using slag replacement. *Cem. Concr. Res.* **2000**, *30*, 465–472. [[CrossRef](#)]
44. Elfmakova, V.; Spiesz, P.; Brouwers, H.J.H. Determination of the chloride diffusion coefficient in blended cement mortars. *Cem. Concr. Res.* **2015**, *78*, 190–199. [[CrossRef](#)]
45. Dalton, R. US researchers fear job losses from privatization drive. *Nature* **2003**, *424*, 478. [[CrossRef](#)]
46. Alafogianni, P.; Dassios, K.; Tsakiroglou, C.D.; Matikas, T.E.; Barkoula, N.M. Effect of CNT addition and dispersive agents on the transport properties and microstructure of cement mortars. *Constr. Build. Mater.* **2019**, *197*, 251–261. [[CrossRef](#)]

47. Dassios, K.G.; Alafogianni, P.; Antiohos, S.K.; Leptokaridis, C.; Barkoula, N.-M.; Matikas, T.E. Optimization of sonication parameters for homogeneous surfactant-assisted dispersion of multiwalled carbon nanotubes in aqueous solutions. *J. Phys. Chem. C* **2015**, *119*, 7506–7516. [[CrossRef](#)]
48. Dalton, R. Museum trustees quit after row over sale of artefacts. *Nature* **2003**, *424*, 360. [[CrossRef](#)] [[PubMed](#)]
49. Dalton, R. Ants join online colony to boost conservation efforts. *Nature* **2003**, *424*, 242. [[CrossRef](#)] [[PubMed](#)]
50. ASTM C1202-97—*Standard Test Method for Electrical Indication of Concrete's Ability to Resist Chloride Ion Penetration*; ASTM International: West Conshohocken, PA, USA, 1997.
51. ASTM B117-16—*Standard Practice for Operating Salt Spray (Fog) Apparatus*; ASTM International: West Conshohocken, PA, USA, 2016.
52. Papadopoulos, M.P.; Apostolopoulos, C.A.; Alexopoulos, N.D.; Pantelakis, S.G. Effect of salt spray corrosion exposure on the mechanical performance of different technical class reinforcing steel bars. *Mater. Des.* **2007**, *28*, 2318–2328. [[CrossRef](#)]
53. Crank, J. *The Mathematics of Diffusion*, 2nd ed.; Clarendon Press: Oxford, UK, 1975.
54. ASTM C1609/C1609M-05—*Standard Test Method for Flexural Performance of Fiber-Reinforced Concrete (Using Beam with Third-Point Loading)*; ASTM International: West Conshohocken, PA, USA, 2005.
55. Alafogianni, P.; Dassios, K.; Farmaki, S.; Antiohos, S.K.; Matikas, T.E.; Barkoula, N.M. On the efficiency of UV-vis spectroscopy in assessing the dispersion quality in sonicated aqueous suspensions of carbon nanotubes. *Colloids Surf. A Physicochem. Eng. Asp.* **2016**, *495*, 118–124. [[CrossRef](#)]
56. Nam, I.W.; Choi, J.H.; Kim, C.G.; Lee, H.K. Fabrication and design of electromagnetic wave absorber composed of carbon nanotube-incorporated cement composites. *Compos. Struct.* **2018**, *206*, 439–447. [[CrossRef](#)]
57. Jiang, S.; Zhou, D.; Zhang, L.; Ouyang, J.; Yu, X.; Cui, X.; Han, B. Comparison of compressive strength and electrical resistivity of cementitious composites with different nano- and micro-fillers. *Arch. Civ. Mech. Eng.* **2018**, *18*, 60–68. [[CrossRef](#)]
58. Song, H.-W.; Lee, C.-H.; Ann, K.Y. Factors influencing chloride transport in concrete structures exposed to marine environments. *Cem. Concr. Compos.* **2008**, *30*, 113–121. [[CrossRef](#)]



© 2019 by the authors. Licensee MDPI, Basel, Switzerland. This article is an open access article distributed under the terms and conditions of the Creative Commons Attribution (CC BY) license (<http://creativecommons.org/licenses/by/4.0/>).